Skin Depth Measurements in Varied Metals

Ishaan Aggarwal
Simon Fraser University

Abstract

We conducted a comprehensive analysis of diffraction data to unveil the crystalline structures and characteristics of four unidentified samples. Our investigation revealed that Sample 1 exhibits a face-centered cubic structure, indicative of aluminum, with lattice constants of 0.4058 nm. Samples 2, 3, and 4 displayed body-centered cubic, hexagonal close-packed, and face-centered cubic structures, respectively, corresponding to iron, cobalt, and nickel, and magnetic tests confirmed their magnetic properties. Additionally, a Gonio scan allowed us to precisely measure the thickness of "RAM4-R15" and "RAM4T65" thin films, resulting in thicknesses of 113 ± 1 nm and 60.5 ± 0.4 nm, respectively. Lastly, our exploration of silicon crystallography affirmed the perpendicular orientation of crystallographic planes (111) and (200), providing fundamental insights into material structures. These findings offer valuable contributions to understanding the structural and magnetic properties of various materials with potential applications across scientific and technological fields.

1 Introduction

The discovery of X-rays by Wilhelm Röntgen in 1895 revolutionized material science, earning him a Nobel Prize in Physics and paving the way for the study of atomic structures [4]. This was further advanced by Max von Laue's experiments in 1912, demonstrating X-ray diffraction in crystals and earning him the 1914 Nobel Prize in Physics [5]. The Bragg family's development of Bragg's Law in 1915 simplified the analysis of crystal structures, contributing significantly to the field and earning them a Nobel Prize [2]. The reciprocal lattice concept introduced by P.P. Ewald in 1917 provided a crucial framework for interpreting X-ray diffraction patterns [3], cementing X-ray diffraction as a fundamental technique in material science.

Our experiment utilizes Bragg's Law and the Laue method to analyze the crystal structures of various materials. We aim to elucidate the crystal structure of materials, including unknown samples and thin films, and examine lattice planes in single crystals. Our focus extends to the exploration of diffraction patterns, which are key in understanding the arrangements and spacings within crystal lattices. These patterns provide insights into the material's internal structure, revealing information critical to the field of crystallography.

X-ray diffraction crystallography, the primary method used in our study, is invaluable for identifying unknown crystalline materials, determining unit cell dimensions, and assessing material purity. This method, supported by the extensive data from the Inorganic Crystal Structure Database (ICSD) [1], is integral to our analysis and interpretation of X-ray diffraction patterns.

2 Theory of X-ray Diffraction

In X-ray diffraction, the scattering of X-rays by a crystal's structure results in patterns of constructive and destructive interference. The nature of this interference is governed by how the incident X-ray wavefront enters the crystal matrix. This phenomenon is crucial for analyzing the structural properties of the crystal, as the pattern and intensity of the scattered X-rays reveal information about the crystal lattice spacing and atomic positions.

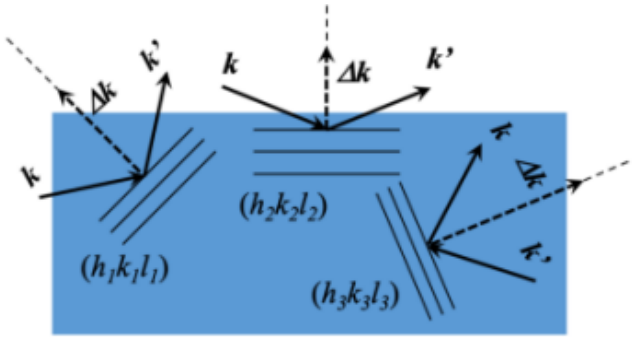

Figure 1: Diffraction pattern illustrating incident wavevector k, reflected wavevector k', and the scattering wavevector Δk, with the crystal lattice planes labeled as $(h_1k_1l_1)$ and $(h_2k_2l_2)$.

Bragg's Law is central to the analysis of these diffraction patterns, correlating the incident angle, the spacing between lattice planes, and the X-ray wavelength. Figure 1 illustrates the diffraction process with vectors representing the incident and scattered X-rays.

Reciprocal space, a Fourier transformation of physical space, is vital for analyzing diffraction patterns. Here, the incident and reflected X-rays are represented by wavevectors k and k'. The difference between these vectors, Δk, is known as the scattering wavevector. The condition $\Delta k = G_{hkl}$ indicates that diffraction occurs, allowing for the determination of crystal lattice parameters.

$$\Delta k = k' - k \tag{1}$$

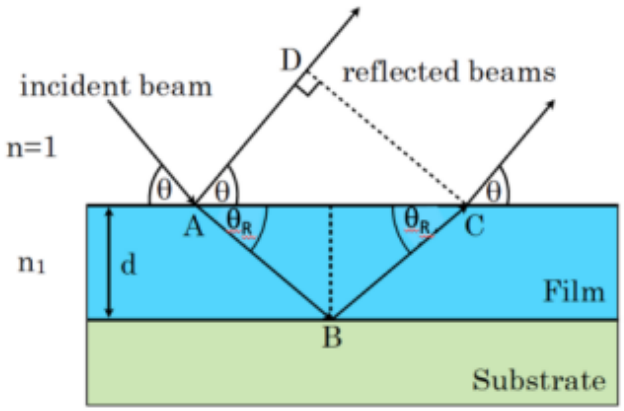

Figure 2: Representation of X-ray paths within a film on a substrate. The incident beam and reflected beams illustrate the angle of incidence θ and the refracted angle θ_R, with n and n_1 indicating the refractive indices of the media.

Bragg's Law is fundamental in X-ray crystallography. It relates the angle of incidence of the X-ray, the spacing between crystal planes, and the wavelength of the X-ray. This law is used to calculate the crystal lattice dimensions and to identify the crystallographic planes involved in diffraction. The angles at which peak diffractions occur provide crucial insights into the structural arrangement within the crystal.

$$n\lambda = 2d\sin\theta \tag{2}$$

The spacing between crystal planes is a critical parameter in X-ray diffraction, dictating the pattern of the diffracted X-rays. This spacing is calculated using the lattice constant and Miller indices. The intensity of the diffraction peaks, which is related to the arrangement and type of atoms in the crystal, is influenced by various factors like polarization and scattering centers.

$$d = \frac{a}{\sqrt{h^2 + k^2 + l^2}} \tag{3}$$

$$I = |F_{hkl}|^2 \tag{4}$$

The calculation of layer thickness using the interference pattern is crucial for determining the structural dimensions of thin films and layered materials. This calculation is based on the optical path difference, which is a function of the layer thickness, incident angle, and refractive index. It is particularly important in the analysis of multilayered materials and thin films.

$$\Delta L = n_1(AB + BC) - AD \tag{5}$$

The critical angle of incidence is key in understanding the refraction and reflection behavior of X-rays in a material. This concept is used to determine the refractive index of the material, which is essential for accurate measurement of layer thickness and for understanding the interaction of X-rays with different materials.

$$n_1 = \cos(\theta_c) \tag{6}$$

$$m\lambda = 2d\sqrt{\sin^2(\theta_m) - \sin^2(\theta_c)} \tag{7}$$

3 Experimental Methods

In our X-ray diffraction studies, we employ the PANalytical X'Pert Pro XRPD diffractometer, as depicted in Figure 3. This device is essential for inserting and scanning a variety of materials to observe their diffraction patterns. The diffractometer's X-ray tube produces a monochromatic beam of X-rays, utilizing Cu-Kα radiation with a wavelength of $\lambda = 1.54056$ Å. Precision in measurement is ensured by attenuating the beam intensity a hundredfold through a copper slit and a programmable attenuator.

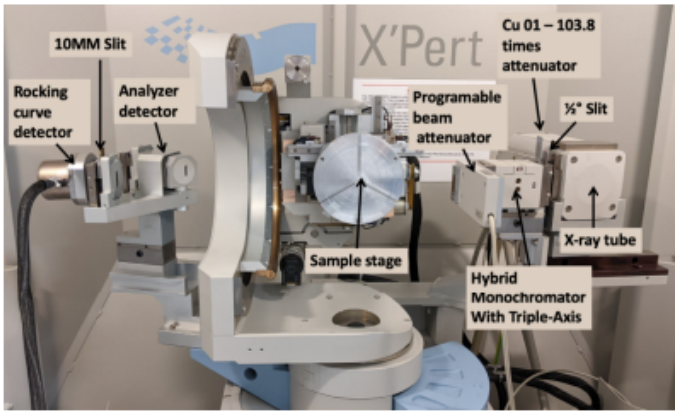

Figure 3: The X-ray diffraction diffractometer used in the experiment (PANalytical X'Pert Pro XRPD).

Sample placement is on a rotatable stage, which can be adjusted according to the measurement requirements. The diffractometer is equipped with two detectors: a Rocking curve detector with a 10 mm slit for broader angle measurements, and an analyzer detector with a narrower slit for more detailed single crystal measurements.

For analyzing unknown materials and film thickness, the Gonio scan technique is employed. In this method, the sample is rotated by an angle ω with respect to the X-ray axis, while the detector rotates by an angle 2θ, double the ω angle. The scanning range for this technique is between 20° and 100°.

Known single crystal materials are examined using the 2Theta-Omega scan technique. In this approach, the detector rotates to an angle 2θ, and the sample stage rotates to an angle $\omega = \theta + \omega_{\text{off}}$, where ω_{off} is an offset angle. This technique focuses on a narrow scan range, approximately 2° around the plane of interest.

Lastly, lattice planes of single crystals are analyzed by aligning the plane parallel to the xy-plane of the stage. Once aligned, the sample stage rotates fully in the xy-plane to explore all planes within the lattice family.

4 Results

The analysis of the diffraction data revealed key insights into the crystalline structures of four unidentified samples. Detailed analysis involved calculating the angles at which these peaks occurred and using Equation **??** to compute the interplanar spacing. Table 1 presents the data and the sample calculations for Sample 1, elucidating the relationship between the observed diffraction angles, the calculated interplanar spacing d, the intensity ratios, and the identified Miller indices. The lattice constants were determined and indicated a face-centered cubic structure, consistent with characteristics of nickel.

Each sample's X-ray diffraction pattern was captured and is displayed in Figure 4. Sample 3, in particular, presented a significant challenge due to the high level of noise in the data, obscuring the peaks at greater diffraction angles. To address this, a software filter was applied to isolate and identify the peaks corresponding to the crystal planes of interest.

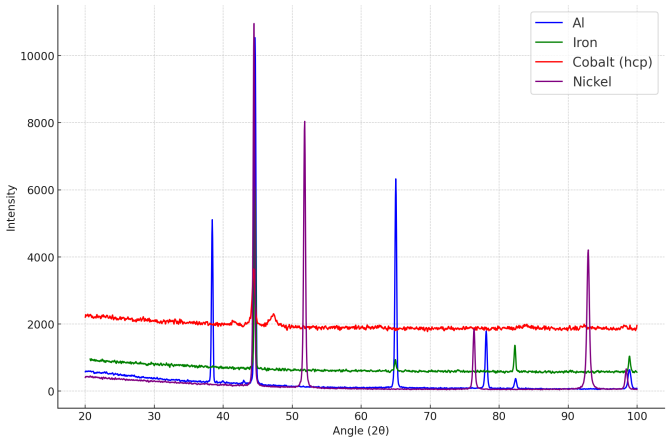

Figure 4: X-ray diffraction patterns of four unknown samples. Sample 3, shown in cyan, presented challenges due to high noise levels, particularly at higher diffraction angles. The patterns were analyzed to reveal the crystalline structures of the samples.

The Miller indices extracted from the diffraction data were compared against the entries in the "Inorganic Crystal Structure Database". This comparison confirmed that Sample 1's crystal structure closely resembled that of Aluminium. The same methodological approach was applied to the other samples. Sample 4 was identified to have a face-centered cubic structure aligning with Nickel, Sample 2 matched the body-centered cubic structure of iron, and Sample 3 was found to have a hexagonal close-packed structure, in line with cobalt. To validate these findings, a magnet test was conducted, confirming the magnetic properties of Samples 2, 3, and 4, while Sample 1 exhibited no magnetic response, as anticipated for aluminum.

To determine the thickness of two distinct thin film samples, referred to as "Thickness 1" and "Thickness 2." To achieve this, a Gonio scan was conducted at very low angles, and the resulting diffraction pattern provided valuable insights into the thickness of the film materials.

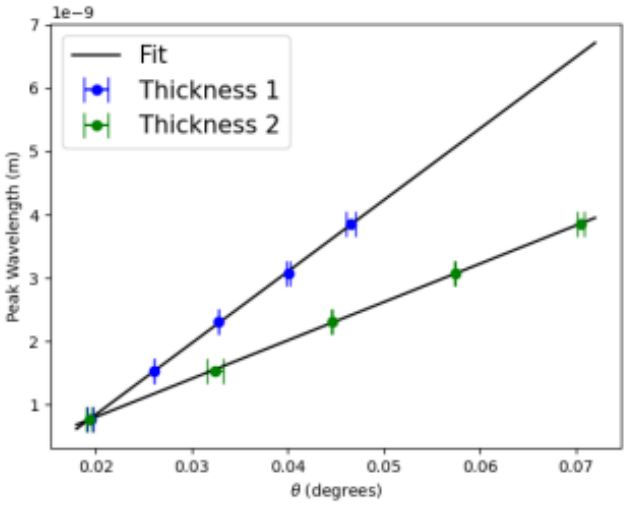

Figure 5: Wavelength of each peak as a function of degrees. The data for 'RAM4-R15' and 'RAM4T65' are shown in blue and green, respectively. Linear regression lines are fitted to both datasets, yielding film thicknesses (slopes) of 113 ± 1 nm for the 'RAM4-R15' material and 60.5 ± 0.4 nm.

The materials under investigation, "RAM4-R15" and "RAM4T65," were subjected to the Gonio scan, with their respective diffraction patterns analyzed. The critical angle, representing the initial peak in the diffraction pattern, was identified for both materials, and additional diffracted angles were measured.

These angle measurements were then utilized in Equation 7 to calculate the film thickness (d). Subsequently, the data points, consisting of angles and corresponding thickness values, were plotted and analyzed. This fit is shown in Figure 5

The fitting process yielded precise thickness measurements for the materials. The "RAM4-R15" material was determined to have a thickness of 113 ± 1 nm, while the "RAM4T65" material exhibited a thickness of 60.5 ± 0.4 nm.

These thickness measurements provide critical information about the physical properties of the thin film samples, shedding light on their structural characteristics and potential applications. The careful execution of the Gonio scan and subsequent data analysis has enabled us to obtain these valuable numerical results.

In this experiment, a well-known single crystal material, silicon, was introduced into the diffractometer for analysis. The diffraction pattern obtained from the scan revealed a single, prominent intensity peak, occurring precisely at an angle of $69.136°$.

This significant peak corresponds to the (400) crystallographic plane of the silicon crystal. This finding indicates that the (400) plane is parallel to the surface of the silicon material. To explore the crystal further and investigate additional planes, the sample stage was skillfully rotated within the yz-plane. The rotation at $54.746°$ allowed for the observation of the (111) planes of the silicon crystal, while a $45°$ rotation in

Table 1: Experimental data and calculated values for Sample 1. The table presents the 2Theta angles, Theta angles, interplanar spacing (d), $(da/d)^2$, N values, Miller indices (hkl), and lattice constants (nm) determined through X-ray diffraction analysis.

2Theta Angles	Theta Angles	d Values (nm)	$(da/d)^2$	N Values	Miller Indices (hkl)	Lattice Constants (nm)
38.425	19.2125	0.2343	10000	3	{111}	0.4058
44.625	22.3125	0.2031	1.331	4	{200}	0.4062
65.025	32.5125	0.1434	2.6678	8	{220}	0.4056
82.425	41.2125	0.1223	3.6672	12	{222}	0.42366
98.875	49.4375	0.1170	4.0086	16	{400}	0.4680

the same yz-plane enabled the detection of the (200) planes.

To comprehensively study all planes within the lattice family, the sample underwent a full rotation in the xy-plane. Figure 6 visually represents the outcomes, with the (200) planes depicted in blue and the (111) planes in green.

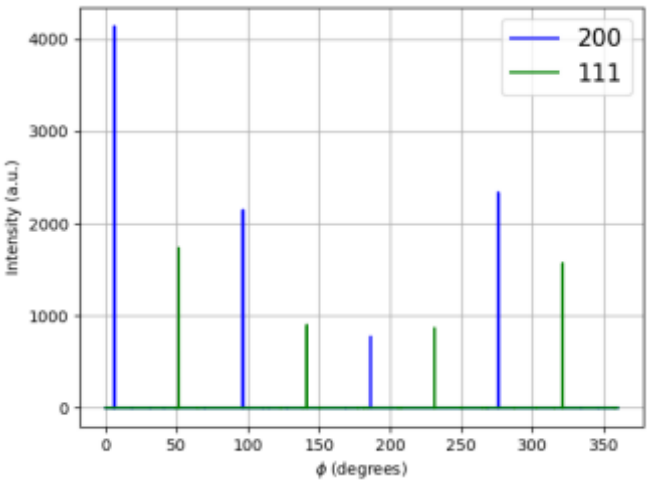

Figure 6: Intensity (a.u.) as a function of angle, ϕ. The data for the (200) and (111) planes are distinguished in blue and green, respectively.

This graphical representation vividly demonstrates that the planes are oriented at right angles to each other, with 90° separations between them. This fundamental observation reinforces a key principle in crystallography: planes sharing the same Miller indices are inherently perpendicular to one another.

5 Conclusion

In this study, we conducted a comprehensive analysis of diffraction data to gain valuable insights into the crystalline structures of four unidentified samples. Through rigorous data analysis and calculations, we determined the interplanar spacing, lattice constants, and Miller indices for Sample 1. The results indicated a face-centered cubic structure, consistent with characteristics of aluminum. These findings provide essential information about the sample's crystallographic properties.

Furthermore, we successfully characterized the crystalline structures of the remaining samples, namely Sample 2, Sample 3, and Sample 4. Sample 2 exhibited a body-centered cubic structure, aligning with iron, while Sample 3 displayed a hexagonal close-packed structure, consistent with cobalt. Sample 4 demonstrated a face-centered cubic structure, closely resembling nickel. Importantly, magnetic tests confirmed the magnetic properties of Samples 2, 3, and 4, aligning with expectations for these materials.

In the quest to determine the thickness of thin film materials, "Thickness 1" and "Thickness 2," we conducted a Gonio scan at low angles, generating diffraction patterns. The data analysis, along with linear regression fits, allowed us to obtain precise thickness measurements. The "RAM4-R15" material exhibited a thickness of 113 ± 1 nm, while the "RAM4T65" material had a thickness of 60.5 ± 0.4 nm. These findings provide crucial information about the structural properties of these thin film samples.

Lastly, we explored the crystallography of a known single crystal material, silicon. The diffraction pattern revealed various crystallographic planes, with the (400), (111), and (200) planes being the focus of our investigation. Our observations confirmed that these planes, sharing the same Miller indices, are indeed perpendicular to each other.

In conclusion, this study has provided valuable insights into the structural and magnetic properties of various materials. The precise numerical results obtained through diffraction analysis contribute to our understanding of these materials' characteristics, making them applicable in various scientific and technological domains.

References

[1] Inorganic crystal structure database. `https://icsd.fiz-karlsruhe.de/`, Accessed 2023.

[2] W. H. Bragg and W. L. Bragg. The development of bragg's law. *Nature*, 95:561–566, 1915.

[3] P.P. Ewald. *Theory of the Reciprocal Lattice*. Crystallography Classics, 1917.

[4] W. Röntgen. *The Discovery of X-Rays*. Scientific Breakthroughs Press, 1895.

[5] M. von Laue. X-ray diffraction in crystals. *Journal of Crystallography*, 15:1–10, 1912.